Polymorphic Meniscus Convergence for Construction of Quasi-Periodic Assemblies and Networks of Colloidal Nanoparticles

By *Sang-Wook Lee, Seung Chul Park, Yongjun Lim, Byoungho Lee,* and *Sin-Doo Lee**

In the emerging nanotechnology field, which demands the continuous miniaturization and the corresponding increase in the density of integration, the construction of a variety of nanostructures is a prerequisite for the development of advanced functional devices[1,2] as well as for the discovery of new phenomena bridging between the micro- and nanoworld.[3] As one of the most promising routes to the integration of the basic units, colloidal particles of various sizes with diverse and tailored composition have attracted much attention for producing building blocks possessing photonic,[4] electronic,[5] or biochemical functions.[6] For example, based on the dimensionality, three-dimensional (3D) structures of colloidal particles for tuning the band-gaps in photonic crystals, two-dimensional (2D) closed-packed structures for lithographic masks[7] whose resolutions depend primarily on the particle size, and one-dimensional (1D) chains for nanowires[5] have been recently demonstrated. Moreover, network structures of nanoparticles will hold promise of a new class of multifunctional devices ranging from signal transduction, chemical and biological analysis/detection, and materials engineering to energy conversion and storage. Therefore, it is extremely important to establish a reliable and flexible strategy of integrating nanoparticles into a variety of functional networks with the single particle resolution. Spatial arrangements of particles into lines and arrays are typically achieved through colloidal dispersions in liquid crystals,[8,9] field-induced dipole interactions,[5,10] or the physical/chemical confinement of a colloidal suspension within templates.[11,12] Particularly, the template-assisted confinement has been well demonstrated for nanoparticle printing and nanopatterning processes.[13,14] However, such confinement approach requires a high-resolution lithography for defining patterns at a nanometer scale,[11,13] limits the flexibility in network design and the accuracy in particle registration, and/or often involves the insufficient connectivity between the adjacent particles.

Here, we present a generic principle of integrating nanoparticles into quasi-periodic assemblies and networks in particle-level resolution from colloidal solutions on the basis of the polymorphic meniscus convergence (MC) around the air-cavities that are regularly embedded on the templates in an auxiliary substrate. The underlying physics behind our MC methodology relies primarily on front propagation of *multiple* liquid-air interfaces dictated by both evaporation and flow in the flow cell. The basic principle of the polymorphic MC in the flow cell geometry is demonstrated in **Figure 1a**,**b**. The flow cell consists of a hydrophobic auxiliary substrate with templates (top) and a hydrophilic support (bottom) arranged so that the colloidal solution can infiltrate by capillary action only into defined regions between the substrate and support. As a consequence, air-cavities are preferentially formed in the templates as shown in Figure 1a. The geometrical parameters of the flow cell, governing the flow propagation as well as the air-cavity formation, are the cell gap (h) between two substrates, the depth (d), and width (w) of the template. In fact, h plays a primary role on both the formation of the air-cavities and the subsequent MC, determining a layer structure in colloidal assemblies and a lateral dimension of the meniscus, $l \approx h/\tan\theta$ in terms of the contact angle θ (or surface tension) at the planar support, provided that $w > 2l$ and $d >> h$. In the extreme case of $w << 2l$ or $d << h$, no stable air-cavity will be generated in the templates. Note that both w and d in our MC approach are of the order of micrometers not nanometers, and thus a nanoscale lithography is not needed (see *Experimental* in Supporting Information). During the solvent evaporation as shown in Figure 1b, two menisci move toward each other, called the MC, and the nanoparticles are then transported to the region with the plane of mirror symmetry.

In the light of the above idea, we present three different classes of the MC that yield distinct self-assembled structures of nanoparticles such as lines and quasi-periodic networks. A simple route to the construction of colloidal nanowires based on the MC is demonstrated in Figure 1c,d. As shown in Figure 1c, well-defined air-channels (or cavities) were selectively formed in a flow cell ($h \approx 0.9$ μm, $d = 2$ μm). Three phase (air, aqueous suspension, and substrate) contact lines were initially pinned at boundaries of the channels on the auxiliary substrate. During solvent evaporation at ambient atmosphere, two menisci converge (binary MC) through the action of the lateral capillary forces as front propagation proceeds (black arrows in Figure 1d). As a result, the immersed nanoparticles move along the direction of front propagation and arrange themselves into a linear structure due to the binary MC.

We now describe how the concept of the *polymorphic* MC, reflecting the flow symmetry with respect to the templates on an auxiliary substrate, can be used for constructing quasi-periodic network structures of nanoparticles from a colloidal solution. A 4-fold symmetric pattern of a template was selected to determine the dependence of the polymorphic MC on the direction of the flow during solvent evaporation. Air-bubble cavities with

[*] S.-W. Lee, S. C. Park, Dr. Y. Lim, Prof. B. Lee, Prof. S.-D. Lee
School of Electrical Engineering
Seoul National University
Kwanak P.O. Box 34, Seoul 151–600 (Republic of Korea)
E-mail: sidlee@plaza.snu.ac.kr

DOI: 10.1002/adma.201001336

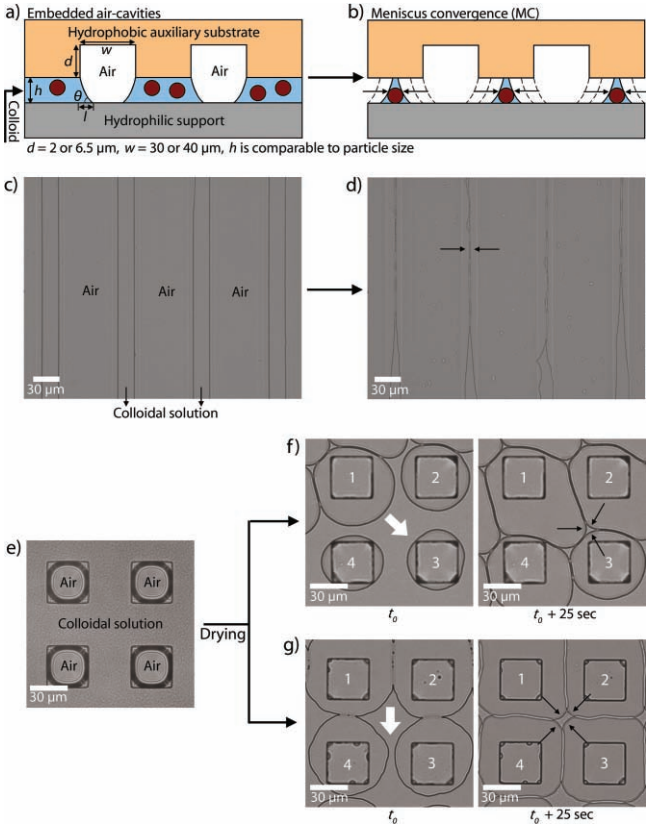

Figure 1. Polymorphic meniscus convergence (MC) for constructing colloidal networks. a,b) Schematic diagrams of the embedded air-cavities (a) in the flow cell and the subsequent MC (b) during solvent evaporation. The geometrical parameters of the flow cell are the cell gap (h) which is related to the lateral dimension (l) of the meniscus as $l \approx h/\tan\theta$, the depth (d), and width (w) of the template, where θ denotes contact angle at the hydrophilic support. c,d) Optical microscopy images showing the air-channel cavities (c) and the subsequent binary MC (d) which yields colloidal nanowires (black arrows). e) Optical microscopy images showing air-bubble cavities embedded in the square-well templates. f) Formation of quasi-hexagonal networks having Y-junctions (three black arrows) through the ternary MC (at t_0 in the left and at t_0 + 25 sec in the right). g) Formation of square-like networks having X-junctions (four black arrows) through the quaternary MC (at t_0 in the left and at t_0 + 25 sec in the right).

the 4-fold symmetry, pinned in a regular array of square-well templates ($h \approx 0.9$ μm, $d = 6.5$ μm), were shown Figure 1e. Consider two directions of the drying-induced flow with respect to the templates, one of which is along the diagonal direction (a white arrow in Figure 1f) and the other the side direction (a white arrow in Figure 1g). In the former, on evaporating the solvent, meniscus 1 moves toward meniscus 3 (initially at t_0 in the left) with joining two menisci of 2 and 4 (at t_0 + 25 sec in the right) as shown in Figure 1f. As a consequence, quasi-hexagonal networks of the nanoparticles having Y-junctions (three black arrows in Figure 1f) were produced through the ternary MC. In the latter, it is clear from Figure 1g that due to the flow symmetry, meniscus 1 and meniscus 2 (at t_0 in the left) become to join 4 and 3 (at t_0 + 25 sec in the right), respectively. Square-like networks having X-junctions (four black arrows in Figure 1g) were formed through the quaternary MC.

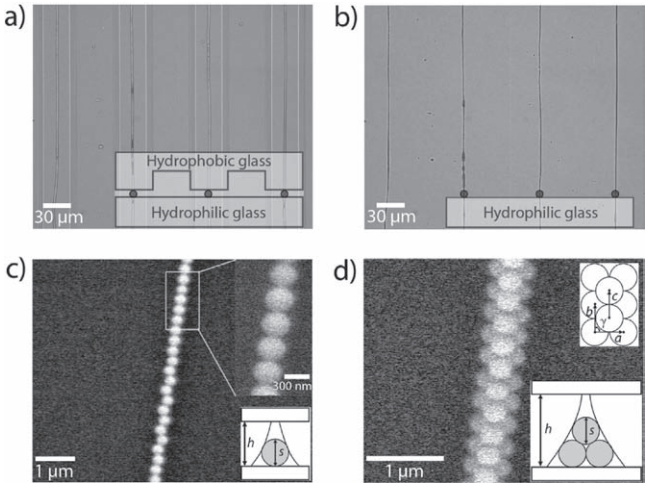

Figure 2. Colloidal nanowires. a,b) The optical microscopy images showing well-preserved colloidal nanowires after the removal of the hydrophobic auxiliary substrate using the predefined wettability contrast. c,d) The SEM images of the colloidal nanowires in a single-layer structure (c) and that in a double-layer structure with $s = 300 \pm 6$ nm (d). Here, h and s denote the cell gap and the particle size, respectively. The lattice constants are denoted by a, b, and c together with the angle of γ.

An example of colloidal nanowires of several millimeters long, constructed in our flow cell, is shown in **Figure 2a** where the solvent was completely evaporated. After the removal of the auxiliary substrate, the nanowires on the hydrophilic support were stable and well preserved as shown in Figure 2b. Note that the length of the nanowire is scalable and extended to an order of the centimeter. A single-layer nanowire and a double-layer nanowire are shown in Figure 2c,d, respectively. The layer formation of colloidal nanoparticles depends primarily on the gap of the flow cell (h) in relative to the particle size (s). For the single-layer formation, the condition of $1 < h/s < 2$ is required. In Figure 2c, $h/s \approx 1.7$ with $h = 500$ nm and $s = 300 \pm 6$ nm. For the double-layer formation, h/s is preferably between 2 and 3. In Figure 2d, $h/s \approx 3$ with $h \approx 900$ nm and $s = 300 \pm 6$ nm, which is consistent with the criterion for the double-layer formation. For nanowires, both a high level of connectivity and a single-particle resolution was naturally achieved through the binary MC as shown in the inset of Figure 2c. The lattice constants of the double-layer structure were measured as $a = 309 \pm 6$ nm, $b = 313 \pm 21$ nm, $c = 312 \pm 10$ nm, and $\gamma = 87° \pm 2°$ (the upper inset in Figure 2d).

For quasi-periodic networks, the direction of the flow during evaporation (a white arrow in **Figure 3a,c**) plays an essential role on the structural symmetry of a unit network, either a hexagon-type (Figure 3a,b) or a square-type (Figure 3c,d), formed through the polymorphic MC. The images observed with a scanning electron microscopy (SEM) indicate that according to the flow symmetry, a Y-junction (Figure 3b) or an X-junction (Figure 3d) is produced through the ternary MC or the quaternary MC, respectively. It was observed that a fast flow generally produces networks with high symmetry but it tends to break the connectivity of the particles. The evaporation rate increases with the curvature of the front meniscus. The front propagation velocity was about 1.5 μm/sec. It is interesting to note that

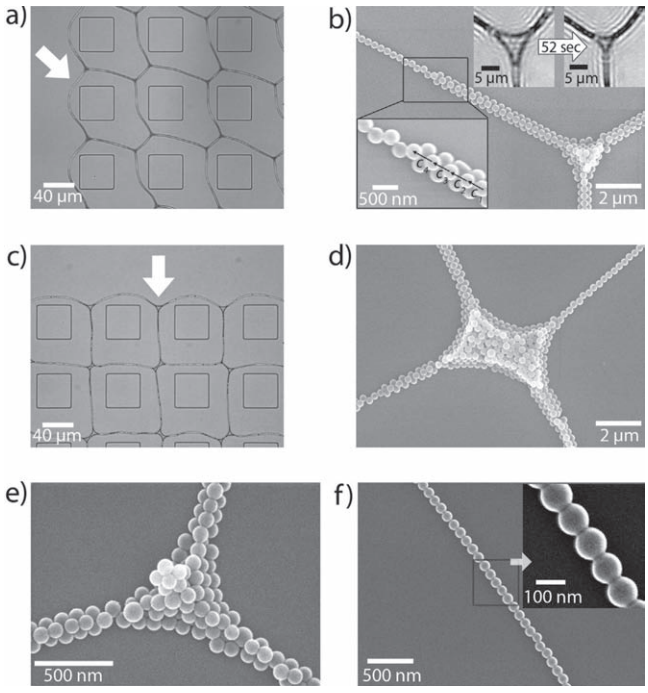

Figure 3. Quasi-periodic networks. a,b) Quasi-hexagonal networks (a) and a Y-junction (b). The upper inset in b shows the ternary MC and the bottom inset in b shows the layer transition. c,d) Square-like networks (c) and an X-junction (d). The white arrow indicates the flow direction (s = 300 ± 6 nm, $h \approx 0.9$ μm). e) The layer transition of particles with $s = 97 \pm 3$ nm in networks moving away from the Y-junction. f) A single-layer nanowire and highly interconnected particles with $s = 97 \pm 3$ nm (the inset of f).

under the condition of $h/s \approx 3$ with $h \approx 900$ nm and $s = 300 \pm 6$ nm, a double-layer nanowire near a junction is transformed into a single-layer nanowire on increasing the lattice constant from $c_1 = 335$ nm ($c_2 = 376$ nm and $c_3 = 396$ nm) to $c_4 = 427$ nm in the transition region (the bottom inset of Figure 3b).

This can be understood from the fact that the surplus particles are accumulated in the vicinity of the junction during the polymorphic MC (the upper inset of Figure 3b) and a more close-packed structure prefers to be formed near the junction than in the branch. It is clear from Figure 3e that for rather small nanoparticles ($s = 97 \pm 3$ nm) or a large ratio of $h/s \approx 4 \sim 5$, a triple-layer junction was observed. The layer transition still exists on moving away from the junction irrespective of the particle size unless strong interparticle interactions other than van der Waals forces are involved. A single-layer nanowire was shown in Figure 3f and highly interconnected nanoparticles in the nanowire were seen in the inset of Figure 3f.

Based on the polymorphic MC described above, we developed a nanoparticle lithography to construct two types of colloid-based nanostructures that are promising for nanophotonic applications. The first is an optical antenna of metallic half-shells and the second is a subwavelength slit of dielectric disks. A linear array of metallic half-shells (denoted by '1' in **Figure 4a,b**) and the counterpart consisting of dielectric disks (denoted by '2' in Figure 4a,c) were fabricated through metal deposition[15,16] on the colloidal chains. The array of dielectric disks shown in Figure 4c was produced by removing nanoparticles after metal deposition. The 3D geometry of metallic half-shell is known to be very useful for directional manipulation of optical responses due to broken symmetry.[4,15] Particularly, our linear array of metallic half-shells in Figure 4b, having the periodicity of a single-particle comparable to the optical wavelength, can serve as an optical antenna. Moreover, the metallic half-shells loaded on the dielectric nanoparticles are capable of enhancing the diffractive coupling of the incident light with traveling surface charge density waves, known as surface plasmon polaritons (SPPs), for generating standing waves along the antenna arm compared to a flat metal nanostructures with the same area.[17] The direction-specific properties of the metallic half-shell antenna were observed through a dark-field microscopy equipped with a dark-field condenser lens having a numerical aperture (NA) of 0.9 for inducing resonant charge oscillation

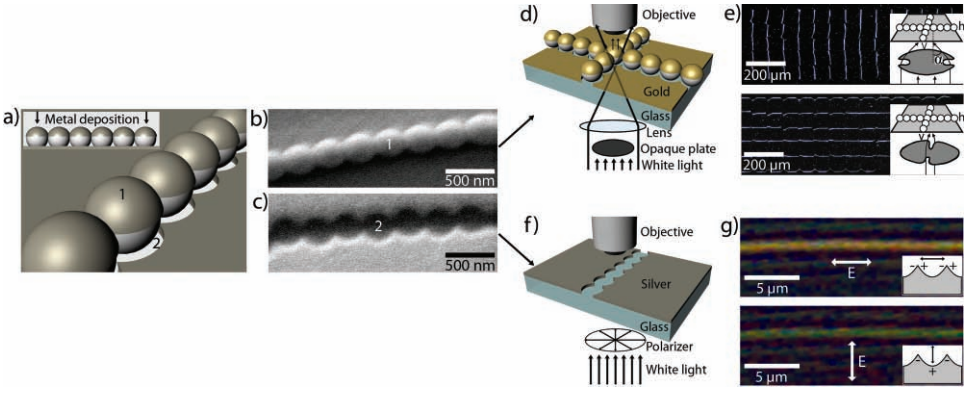

Figure 4. Optical antenna of metallic half-shells and subwavelength slit of dielectric disks. a) Schematic diagrams showing the fabrication of metallic half-shells and the counterpart of dielectric disks through metal deposition (inset) on a colloidal chain. b,c) The SEM images of the fabricated metallic half-shells (label 1 in a and b) and the dielectric disks (label 2 in a and c). d,e) A schematic diagram of dark-field microscopy on optical antenna (d) and the dark-field images (e) showing the direction-specific activation of metallic half-shell antenna through the constructive interference between the induced charge and the SPP charge (inset in e). f,g) A schematic diagram of light transmission through the subwavelength slit of dielectric disks (f) and the optical microscopy images (g) showing the color change (yellowish in the top and greenish in the bottom) of the transmitted light depending on the polarization (white arrow) of illuminated white light. The inset in (g) shows a plasmon oscillation mode for each polarization of light in the slit.

and an objective lens (NA = 0.3) for collecting far-field radiation (Figure 4d). In a crossed linear array of metallic half-shells (Figure 4e), either the vertical nanowire 'v' (top in Figure 4e) or the horizontal nanowire 'h' (bottom in Figure 4e) can be selectively activated by the component of light perpendicular to the corresponding nanowire. In fact, the total charge (q_n) at an edge of the metallic half-shell is the sum of an induced primary charge, $q(w)$, and a SPP charge traveling from the neighboring half-shell (q_{n-1}), that is, $q_n = q(w) + rq_{n-1} \exp(ik_{spp}p)$ where w is frequency of incident light, r is the coupling constant (<1), k_{spp} is the wave vector of the SPP, and p is periodicity. The component of light perpendicular to the nanowire (no parallel component) induces the constructive interference between the primary charge and the SPP. In this case, $k_{spp} = 2\pi/\lambda_{spp}$ and $p = (n + 1/2)\lambda_{spp}$ where $n = 0, 1, 2,\ldots$ and λ_{spp} is the wavelength of SPP.[18] As a consequence, $q_n = -q_{n-1} = q(w)/(1-r)$ which is greater than $q(w)$, indicating that the enhancement of the charge oscillation occurs. On the other hand, the component of light along the nanowire at the incident angle of α to the nanowire 'h' (the upper inset of Figure 4e) induces the destructive interference due to the presence of the parallel component ($k \sin \alpha$) in k_{spp} which leads to a mismatch with the phase of primary dipolar oscillation. Due to the particular complex morphologies of the ordered metallic half-shells,[15,17] our optical antenna would induce a variety of plasmon oscillation modes in response to a broad spectrum of light which is promising especially for biosensing devices through plasmon-coupled fluorescence enhancement.[19] We now demonstrate a subwavelength slit of dielectric disks, having a single-particle width in a sharp-tip geometry, as shown in Figure 4f. Compared to conventional uniform-gap nanoslits,[20] the sharp-tips in our slit allow the coupling of the incident light having an arbitrary polarization with a surface wave propagating within the slit. This will provide a scheme of modulating the wavelength of the transmitted light and the launched SPP on the metal film by means of a polarization variation without modifying the slit geometry.[20] For the measurements, a beam of white light from a broad-band halogen lamp was incident onto the dielectric disk slit as shown in Figure 4f. The color change of the transmitted light (yellowish in the top of Figure 4g and greenish in the bottom in Figure 4g), depending on the polarization state of the input light (denoted by E in Figure 4g), is indicative of strong coupling of light with surface plasmons in our sharp-tip geometry. A plasmon mode for each polarization was shown in the inset of Figure 4g. Owing to the local field enhancement in the sharp-tip, the dielectric disk slit is promising for use in subwavelength waveguides and biomolecular sensors.

In conclusion, the polymorphic MC presented here provides a practical route to construction of 1D and/or 2D quasi-periodic colloidal networks reflecting the flow symmetry around the air-cavities during solvent evaporation. A wide spectrum of colloidal nanostructures including curved nanowires or multi-branch junctions can be generated through modifications of air-cavities with size, shape, spacing, and arrangement. Moreover, incorporation of different classes of materials such as nanotubes and nanowires into colloidal systems will lead to more functional flexibility for highly integrated devices.

Supporting Information

Supporting Information is available online from Wiley InterScience or from the author.

Acknowledgements

This work was supported by the National Research Foundation of Korea and the Ministry of Education, Science and Technology of Korea through the Creative Research Initiative Program (2009–0063599). SDL would like to thank Jein Medical Center for financial support in part.

Received: April 14, 2010
Published online:

[1] A. D. Dinsmore, M. F. Hsu, M. G. Nikolaides, M. Marquez, A. R. Bausch, D. A. Weitz, *Science* **2002**, *298*, 1006.
[2] B. Pokroy, S. H. Kang, L. Mahadevan, J. Aizenberg, *Science* **2009**, *323*, 237.
[3] E. Dressaire, R. Bee, D. C. Bell, A. Lips, H. A. Stone, *Science* **2008**, *320*, 1198.
[4] N. A. Mirin, N. J. Halas, *Nano Lett.* **2009**, *9*, 1255.
[5] K. D. Hermanson, S. O. Lumsdon, J. P. Williams, E. W. Kaler, O. D. Velev, *Science* **2001**, *294*, 1082.
[6] M. M. Baksh, M. Jaros, J. T. Groves, *Nature* **2004**, *427*, 139.
[7] J. C. Hulteen, R. P. V. Duyne, *J. Vac. Sci. Technol. A* **1995**, *13*, 1553.
[8] I. Musevic, M. Skarabot, U. Tkalec, M. Ravnik, S. Zumer, *Science* **2006**, *313*, 954.
[9] P. Poulin, H. Stark, T. C. Lubensky, D. A. Weitz, *Science* **1997**, *275*, 1770.
[10] J. Ge, Y. Yin, *Adv. Mater.* **2008**, *20*, 3485.
[11] Y. Cui, M. T. Bjork, J. A. Liddle, C. Sonnichsen, B. Boussert, A. P. Alivisatos, *Nano Lett.* **2004**, *4*, 1093.
[12] J. Aizenberg, P. V. Braun, P. Wiltzius, *Phys. Rev. Lett.* **2000**, *84*, 2997.
[13] T. Kraus, L. Malaquin, H. Schmid, W. Riess, N. D. Spencer, H. Wolf, *Nat. Nanotechnol.* **2007**, *2*, 570.
[14] W. Cheng, N. Park, M. T. Walter, M. R. Hartman, D. Luo, *Nat. Nanotechnol.* **2008**, *3*, 682.
[15] H. Takei, *J. Vac. Sci. Technol. B* **1999**, *17*, 1906.
[16] L. Y. Wu, B. M. Loss, L. P. Lee, *Nano Lett.* **2009**, *9*, 1956.
[17] A. I. Maaroof, M. B. Cortie, N. Harris, L. Wieczorek, *Small* **2008**, *4*, 2292.
[18] Y. Alaverdyan, B. Sepulveda, L. Eurenius, E. Olsson, M. Kall, *Nat. Phys.* **2007**, *3*, 884.
[19] C. Farcau, S. Astilean, *Appl. Phys. Lett.* **2009**, *95*, 193110.
[20] H. W. Kihm, K. G. Lee, D. S. Kim, J. H. Kang, Q.-H. Park, *Appl. Phys. Lett.* **2008**, *92*, 051115.